Ancient TL

www.ancienttl.org · ISSN: 2693-0935

Choi, J., Duller, G. and Wintle, A., 2006. *Analysis of quartz LM-OSL curves.* Ancient TL 24(1): 9-20.
https://doi.org/10.26034/la.atl.2006.390

Analysis of quartz LM-OSL curves

J.H. Choi[1,2], G.A.T. Duller[2] and A.G. Wintle[2]

1. Geochronology Team, Korea Basic Science Institute, Daejeon 305-333, South Korea
2. Institute of Geography and Earth Sciences, University of Wales, Aberystwyth, SY23 3DB, UK

(Received 22 December 2005; in final form 15 May 2006)

Abstract

Measurement of the optically stimulated luminescence signal during linear ramping of the stimulation power (LM-OSL) is a useful and efficient method for separating constituent OSL components, and for detailed investigation of the luminescence properties of each component. However, the practical procedures for the analysis of the quartz LM-OSL signal have been largely ambiguous in previous publications. In this study, we discuss various aspects of the analysis of quartz LM-OSL curves. This includes the measurement of background count rate, deconvolution of the LM-OSL curves using commercially available software, derivation of detrapping probabilities from the fitting results, and the identification and characterisation of each OSL component based upon the photoionisation cross-sections derived from these values.

Introduction

A decade ago, Bulur (1996) introduced an innovative method of measuring optically stimulated luminescence (OSL) which is now widely known as LM-OSL (Linearly Modulated OSL). The LM-OSL signal is observed by linearly increasing the stimulation power of the light source during measurement, and it has many advantages over continuous wave OSL (CW-OSL) measured with constant stimulation power. By ramping the stimulation power from zero to a particular value (usually the maximum power of the light source), the OSL signal appears as a series of peaks; each peak represents a component of the OSL signal with a particular physical parameter, namely the photoionisation cross-section. The LM-OSL signal allows more effective and accurate characterisation of each OSL component than the CW-OSL signal, and thus, LM-OSL can be used as an essential tool for understanding processes giving rise to OSL and improvement of the optical dating procedure based on measurement of CW-OSL.

Recently, various physical aspects of OSL components (such as sensitivity, dose response, thermal stability, and recuperation) have been investigated using LM-OSL signals from single and multiple quartz grains (Bulur et al., 2000, 2002; Jain et al., 2003; Kuhns et al., 2000; Singarayer, 2002; Singarayer and Bailey, 2003). In addition, LM-OSL signals have been used to identify the cause of problems in dating sediments (equivalent dose estimation) using quartz grains (Choi et al., 2003a and b; Tsukamoto et al., 2003). Singarayer and Bailey (2003, 2004) showed that one of the slow components (the slowest component they observed) saturated at much higher doses (> 1000 Gy) than the fast component that usually dominates the initial part of the CW-OSL signal; this component has potential for dating old samples of around 1 Ma. All these studies make use of LM-OSL signals and require the separation and identification of the different OSL components; this can be achieved, in principle, by mathematical deconvolution of LM-OSL curves. However, the process of fitting components to the LM-OSL curve and the derivation of trap parameters for each component are somewhat ambiguous in the earlier publications.

In this paper, we present the process of fitting components to the LM-OSL curve obtained from multi-grain single aliquots of quartz, using commercially available software and the derivation of useful trap parameters from the fitting results. The procedures are applied to two sedimentary quartz samples that have very different LM-OSL characteristics.

Samples and experimental details

Quartz grains extracted from a fluvial sediment from the Kenyan Rift Valley (lab code ER4) and an aeolian dune sand from Tasmania, Australia (lab code TNE9517) were used in this study. The quartz fraction of 150-250 μm diameter grains was recovered by density separation and sieving, and purified through sequential use of 10 vols H_2O_2, 10% HCl, and 40% HF. The detailed luminescence characteristics of these two samples have been

reported elsewhere (Choi et al., in press; Duller and Augustinus, in press).

Quartz OSL was measured using an automated luminescence measurement system (Risø TL/OSL-DA-15), which is equipped with a $^{90}Sr/^{90}Y$ beta source delivering 0.11 Gy·s^{-1} to the sample position. Quartz OSL was stimulated using blue LED arrays (470 ± 30 nm) with a green long-pass GG-420 filter in front of the LEDs, and the stimulation temperature was 125°C. Photon detection was by an EMI9235QA photomultiplier tube through 7.5 mm thickness of Hoya U-340 filter. Quartz LM-OSL signals were measured by linearly ramping the stimulation power of the blue-LEDs from 0 to 90 % (~ 30 mW·cm^{-2}) of full power over a period of 3600 s with the photon counts being collected every 4 s. The quartz grains were mounted over an area of 8 mm diameter on 9.7 mm diameter aluminium discs using silicone oil (~ 1600 grains per aliquot).

Deconvolution of the LM-OSL curves was performed using commercial software SigmaPlot^{TM} (ver. 7), which employs the Marquardt-Levenberg algorithm for linear and non-linear fitting.

Deconvolution of LM-OSL curves

Background subtraction and testing the linearity of the increase in stimulation power

Before fitting LM-OSL curves, it is important to consider the background count rate while ramping the stimulation power. In order to measure the background, 5 blank aluminium discs (coated with a thin silicone oil layer, but without quartz grains on top of it) were prepared and the photon count rate was measured whilst increasing the stimulation power of the blue LEDs from 0 to 30 mW·cm^{-2} for 3600 s (the disc was held at a constant temperature of 125°C). The background count rates from all the blank discs were found to be dependent upon the stimulation light intensity; the background count rates increased with increasing stimulation light intensity. The average of the background data from five aliquots is depicted as open circles in Fig. 1(a).

Two further experiments were performed under the same stimulation conditions. In the first, aluminium discs were used without silicone spray, and in the second, stainless-steel discs (with and without silicone spray) were used; similar data sets (not shown here) were obtained. Thus, it was concluded that the increase of the background count rate with increasing stimulation light intensity, as shown in Fig. 1(a), is the result of stimulation light breaking through the Hoya U-340 detection filter and arriving at the photomultiplier tube.

The point-by-point average of the background data could be best fitted using a quadratic function ($y = 294 + 0.04921\ x + 0.00003239\ x^2$, solid line in Fig. 1(a)) with an R^2 value of 0.998. If the background is solely related to the stimulation light, the intensity of which is increased linearly, the background should increase linearly. A possible explanation for the non-linearity is a slight change in wavelength of the LED emission as the power is increased, allowing more photons to pass through the Hoya U-340 filter, though this hypothesis has not been tested.

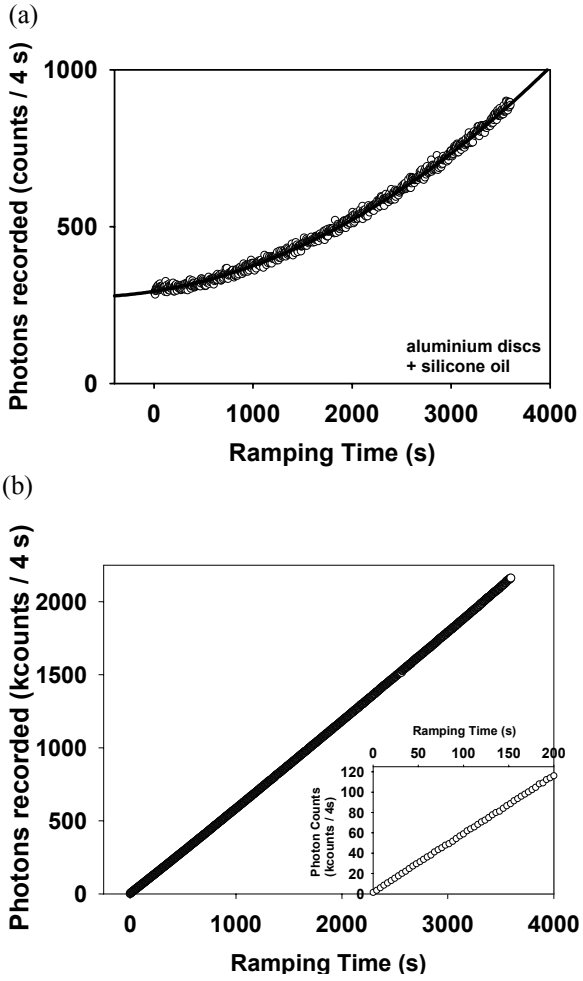

Figure 1: *(a) Background count rate as measured on a blank disc (aluminium discs with silicone spray, but no quartz grains) with the standard U-340 filters. The average of the background data can be best fitted using a quadratic function. (b) Photon counts measured while ramping the blue LED power from 0 to 90% over a period of 3600s. For this measurement the U-340 filters were removed and replaced by an opaque disc with a pin hole and three neutral density filters. The inset shows the same data over the interval from 0 to 5% of full power in the first 200 s.*

For subsequent LM-OSL measurements, we take the quadratic fit derived above as the background, and all the LM-OSL curve fittings described in this paper are performed after subtraction of this background from the measured data sets.

Another critical test to make prior to LM-OSL measurement is that the increase in the intensity of the light emitted by the blue LEDs is linear during the measurement. The mathematics described by Bulur (1996) is based upon the assumption that this is the case. This was tested by removing the U-340 filters and replacing them with an opaque disc in which a pin hole was placed. Three semi-silvered neutral density filters (ND3.0, ND1.0 and ND1.0) were then added to attenuate the signal by a factor of 100,000 so that the photomultiplier was not blinded. A blank aluminium disc was placed on the carousel. In this way, the photomultiplier could be used to directly measure the intensity of the blue LEDs during an LM-OSL procedure. Fig. 1(b) shows the photon counts measured during the 3600 s of an LM-OSL procedure in which the blue LEDs were ramped from 0 to 90% of full power. Fitting a straight line to this data gives an R^2 value of 0.9999. The inset to Fig. 1(b) shows that the increase is linear even over the range from 0 to 5% of full power. (Please note that caution is required when making this measurement to avoid blinding, and permanently damaging, the photomultiplier tube by exposing it to the blue LEDs without appropriate shielding).

Equations for use in SigmaPlot™

The LM-OSL curves were obtained by stimulating the natural quartz grains of samples TNE9517 and ER4 (one aliquot for each sample) with increasing stimulation light intensity from 0 to 30 mW·cm^{-2} for 3600 s at 125°C. The photon count data sets were transferred to the graphics software (SigmaPlot™), the background subtracted and the LM-OSL vs. ramping time plots used for curve fitting (Fig 2). The simplest form of the equation governing the LM-OSL curve has been given in Bulur et al. (2002):

$$L(t) = n_0\, b\, (t/P) \exp(-bt^2/2P) \qquad \text{(Eqn. 1)}$$

where L(t) is the luminescence intensity as a function of time (t), n_0 is the number of trapped electrons, P is the total stimulation time, b is the detrapping probability, which is proportional to the photoionisation cross-section (σ) and the maximum stimulation light intensity (I_0) with $b = \sigma I_0$ (see Appendix 1 for example calculations).

The number of OSL components has been shown to vary from sample to sample; Jain et al. (2003) identified 6 OSL components from 9 sedimentary quartz samples, but Singarayer and Bailey (2003) reported that most of the sedimentary quartz samples that they analysed had 5 components. Choi et al. (in press) also showed that more than 80% of the samples investigated in their study have 5 components, whereas they identified only 3 OSL components from the well-studied sedimentary quartz WIDG8 from western Australia. However, the number of components in these previous studies is based on the LM-OSL curves observed from multi-grain aliquots, whereas others have shown that the number of components varies from grain-to-grain when measurements are made on individual grains (Bulur et al., 2002; Yoshida et al., 2003).

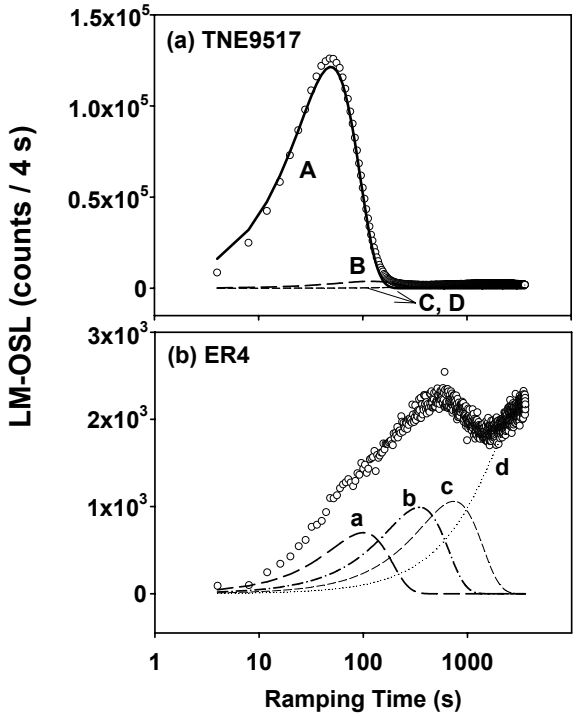

Figure 2: *Separation of quartz LM-OSL signals by mathematical fitting with commercially available software (SigmaPlot™). Both (a) an aeolian sample from Tasmania (TNE9517) and (b) a fluvial sample from Kenya (ER4) could be separated into 4 components, but having a different selection of photoionisation cross-sections (Table 5).*

Although the value of σ (cm^2) is the fundamental property, b (s^{-1}) is more convenient for use in the software package. On the basis of Eqn. 1, the following form (Eqn. 2) was entered into the fitting program of the software ("Regression Wizard" in SigmaPlot™).

Relative σ		N = 3	b_N / b_1	N = 4	b_N / b_1	N = 5	b_N / b_1	N = 6	b_N / b_2
σ_F / σ_F = 1.0	n_1	9.988×10^6	1.0	9.870×10^6	1.0	5.212×10^6	1.0	6.967×10^1	1.2×10^5
	b_1	1.468		1.482		1.482		1.735×10^5	
σ_M / σ_F = 0.2	n_2	7.917×10^5	0.1	7.370×10^5	0.2	4.659×10^6	1.0	5.887×10^6	1.0
	b_2	0.1584		0.2580		1.482		1.482	
σ_{S1} / σ_F = 0.06	n_3	8.935×10^6	0.001	8.074×10^5	0.01	7.370×10^5	0.2	3.983×10^6	1.0
	b_3	0.0010		0.0107		0.2580		1.482	
σ_{S2} / σ_F = 0.01	n_4			9.118×10^6	0.001	8.074×10^5	0.01	7.370×10^5	0.2
	b_4			0.0008		0.0107		0.2580	
σ_{S3} / σ_F = 0.001	n_5					9.118×10^6	0.001	8.074×10^5	0.01
	b_5					0.0008		0.0107	
σ_{S4} / σ_F = 0.0001	n_6							9.118×10^6	0.001
	b_6							0.0008	
	R^2	0.999		0.999		0.999		0.999	

Notes:
Relative σ values are from Jain et al. (2003). N is the number of OSL components in the fitting equation (Eqn. 2). Initial b_N values for fitting were derived from Jain et al. (2003) (see text). Initial n_N was set to 10^5 and n_N and b_N were constrained to be $n_N > 0$, $b_N > 0$. The number of iterations, step size, and tolerance were set to 10^5, 10^2 and 10^{-500}, respectively. Shaded boxes represent imaginary components with very high *b* and low *n* values (see text for details).

Table 1: *Output parameters of LM-OSL curve fitting of sample TNE9517 with different numbers of OSL components (initial b values taken from Jain et al. (2003), listed in order of descending value)*

$$f = n_1 b_1 (t/P) \exp(-b_1 t^2/2P) + n_2 b_2 (t/P) \exp(-b_2 t^2/2P) + n_3 b_3 (t/P) \exp(-b_3 t^2/2P) + n_4 b_4 (t/P) \exp(-b_4 t^2/2P) + n_5 b_5 (t/P) \exp(-b_5 t^2/2P) + \ldots\ldots\ldots\ldots + n_N b_N (t/P) \exp(-b_N t^2/2P) \quad \text{(Eqn. 2)}$$

where P, the total stimulation time, was fixed as 3600 s in this experiment, and the values n_N (number of trapped electrons) and b_N (detrapping probability) are those obtained through mathematical fitting.

One way of seeing whether the individual values of b (and thus σ, since $b = \sigma I_0$) have the same relative behaviour as has been found by others, is to compare the ratios of the parameter b for each of the N components. These can also be compared with the relative values of σ published by others. We have chosen to compare our ratios of b values with the ratios for σ values of the components reported by Jain et al. (2003). The latter ratios can be seen in the furthest left column of Table 1. The data sets for TNE9517 and ER4 are available on the journal web page as described in Appendix 2.

Fitting LM-OSL curve for TNE9517
The LM-OSL curve for sample TNE9517 was fitted with a varying number of constituent OSL components (3, 4, 5 and 6 components; N = 3, 4, 5, 6 in Eqn. 2), and the results are summarised in Table 1. The initial n_N values were set to be 100000 and the initial values for b_N were based on the values of σ given by Jain et al. (2003), but for a maximum power of 30 mW·cm^{-2}, rather than 47 mW·cm^{-2} as used by Jain et al. (2003). For N=3 components, these were σ_F, σ_M and σ_{S1} for the fast, medium and slow1 components with initial values of 2.32×10^{-17}, 5.59×10^{-18} and 1.33×10^{-18} (cm^2), respectively, giving rise to b values of 1.65, 0.396, and 0.0943 (s^{-1}). The value of P in Eqn. 2 was fixed as 3600 s, and the maximum number of iterations was 10^5 with a step size of 10^2. The tolerance was set to 10^{-500} in order that the fitting process stops when the absolute value of the difference between the norm of the residual (square root of the sum of the squares of the residuals by definition), from one iteration to the next, is less than 10^{-500}. For N=4, 5 and 6, values of b were calculated from the data of Jain et al. (2003) giving 0.0147, 0.0015 and 0.0002 (s^{-1}) for slow2, slow3 and slow4.

From Table 1, it can be seen that the values of b_1, b_2 and b_3 obtained when N was set to 3 are similar, but not identical, to the values entered at the start of the iteration. The ratios of b_2 / b_1 and b_3 / b_1 are similar to the equivalent ratios of σ_M / σ_F and σ_{S1} / σ_F, using the values of Jain et al. (2003). Fitting of 3 components was good as shown by the R^2 value being 0.999.

Similar results were obtained for N=4 when adding in the extra components (slow2 for N=4). The values of b_1 were very similar for N=3 and N=4, and those for b_2 and b_3 were not dissimilar. For N=5 (additionally adding in the b value for slow3), it can be seen from the repetition of 1.482 as both the calculated b_1 and b_2 values, and the simultaneous division of n between n_1 and n_2, that the software has created two almost identical LM-OSL signal components. This implies redundancy in the number of components, and the conclusion is that only 4 components are present in the TNE9517 signal in Fig. 2(a). For N=6 (additionally adding in the b value for slow4) then the same redundancy is seen by the identical values found for b_2 and b_3. In addition, for N=6, an imaginary component, with a very high value of b ($b_1 = 1.735 \times 10^5$) and a very low value of n ($n_1 = 6.967 \times 10^1$) can be seen (shaded box in Table 1). This result also confirms the conclusion reached for N=5, namely that TNE9517 LM-OSL is well represented by 4 components. Thus the signals are probably the fast, medium, slow2 and slow3. In addition, the relative values of b, shown as b_i / b_1, are similar to the ratios for σ_i / σ_F for the photoionisation cross-sections of Jain et al. (2003).

Fitting LM-OSL curve for ER4

The same approach was taken for ER4 (Fig. 2(b)), starting by entering the values of b for the fast, medium and slow1 components for N=3. In this case, the fit was not good, with $R^2 = 0.841$, and the values obtained were not similar to those entered (Table 2). When fitting for N=4 (adding in b for slow2), the use of 4 components resulted in a better fit ($R^2 = 0.915$). However, N=5 (adding in b for slow3) resulted in a worse fit, owing to the calculation of 3 components with very high b values (shaded part of Table 2). For N=6, the 4 components found for N=4 were again calculated, together with two imaginary components that had no effect on the fitting ($R^2 = 0.915$, as for N=4). This again confirms that ER4 has 4 components, as previously suggested by Choi et al. (in press). In this case, the components are thought to be the medium, slow2, slow3 and slow4 components of Jain et al. (2003) on the basis of the ratios of the b values compared with the ratios of σ. In no calculation was a fast component identified.

Relative σ		N = 3	b_N / b_1	N = 4	b_N / b_1	N = 5	b_N / b_4	N = 6	b_N / b_3
σ_M / σ_M = 1.0	n_1	2.659×10^5	1.0	1.153×10^5	1.0	3.814×10^4	1.2×10^8	5.009×10^{-5}	1.7×10^9
	b_1	0.1224		0.3607		1.832×10^6		6.159×10^8	
σ_{S1} / σ_M = 0.24	n_2	1.478×10^6	0.09	5.647×10^5	0.08	1.615×10^{-7}	2.6×10^6	2.702×10^{-5}	3.2×10^5
	b_2	0.0105		0.0302		4.014×10^4		1.138×10^5	
σ_{S2} / σ_M = 0.04	n_3	1.084×10^7	0.003	1.292×10^6	0.02	3.072×10^4	2.2×10^5	1.153×10^5	1.0
	b_3	0.0004		0.0066		3.409×10^3		0.3607	
σ_{S3} / σ_M = 0.004	n_4			1.215×10^7	0.0008	1.461×10^6	1.0	5.647×10^5	0.08
	b_4			0.0003		0.0155		0.0302	
σ_{S4} / σ_M = 0.0005	n_5					9.920×10^6	0.03	1.292×10^6	0.02
	b_5					0.0005		0.0066	
	n_6							1.215×10^7	0.0008
	b_6							0.0003	
	R^2	0.841		0.915		0.402		0.915	

Notes

Relative σ values are from Jain et al. (2003). N is the number of OSL components in the fitting equation (Eqn. 2). Initial b_N values for fitting were derived from Jain et al. (2003) (see text). Initial n_N was set to 10^5 and n_N and b_N were constrained to be $n_N > 0$, $b_N > 0$. The number of iterations, step size, and tolerance were set to 10^5, 10^2 and 10^{-500}, respectively. Shaded boxes represent imaginary components with very high *b* and low *n* values (see text for details).

Table 2: *Output parameters of LM-OSL curve fitting of sample ER4 with different numbers of OSL components (initial b values starting from Jain et al.'s (2003) fast component b values)*

Tests for the fitting of ER4 LM-OSL curve

Since no fast component was found, even though the initial estimate for the first b value (b_1) was given the value for the fast component of Jain et al. (2003), it was expected that the ability to fit components would not be sensitive to the selection of initial b values. In particular, we anticipated that starting with b_1 equal to the value of the medium component of Jain et al. (2003) would also result in the same 4 components. The results from this analysis are given in Table 3. Firstly with N=3, the results were identical to those calculated in Table 2, with the same low value of R^2 (0.841). Increasing the number of components in the same way (by adding in the next smallest value of b), the curve was poorly fitted, with $R^2 = 0.402$ for both N=4 and N=5 and with two or three imaginary components being presented (shaded boxes in Table 3). Thus it seemed impossible to recover more than 3 components or values of b, unlike the situation when starting the calculation with the fast component b value.

The data for ER4 were re-investigated for N=3 and N=4, but using the values obtained from Table 2 (N=4 or N=6 with $R^2 = 0.915$). For N=3, the values of b obtained for the 3 components were the same as had been obtained in both Table 2 and Table 3, with $R^2 = 0.841$ (Table 4). For N=4, the same three components were obtained with $R^2 = 0.841$, but an additional, imaginary, component was calculated (shaded box). The calculation for N=4 was then repeated, but constraining b to lie between 0 and 2, noting that b for the fast component was calculated to be 1.468 (Table 1). Application of this constraint resulted in four b values being obtained, each of which was numerically identical to those obtained in Table 2.

The sensitivity of the fitting algorithm to the choice of the initial values for the fitted parameters was investigated for two synthetic LM-OSL data sets (Appendix 3) where the true values of b and n were known. This showed that while a wide range of initial values resulted in identical final values, there were certain combinations of initial parameters that did not result in the correct values being determined. In these cases, b values that were either very large ($>\sim10^3$) or very small ($<\sim10^{-6}$) were produced. Further work is required to understand the optimum choice of initial starting parameters.

Relative σ		N = 3	b_N / b_1	N = 4	b_N / b_3	N = 5	b_N / b_4
$\sigma_M / \sigma_M = 1.0$	n_1	2.659×10^5	1.0	2.675×10^4	1.6×10^8	1.621×10^{-5}	7.7×10^9
	b_1	0.1224		2.443×10^6		1.188×10^8	
$\sigma_{S1} / \sigma_M = 0.24$	n_2	1.478×10^6	0.09	1.160×10^4	1.9×10^5	9.507×10^{-4}	4.9×10^9
	b_2	0.0105		2.898×10^3		7.521×10^7	
$\sigma_{S2} / \sigma_M = 0.04$	n_3	1.084×10^7	0.003	1.461×10^6	1.0	5.100×10^{-4}	7.9×10^6
	b_3	0.0004		0.0155		1.219×10^5	
$\sigma_{S3} / \sigma_M = 0.004$	n_4			9.920×10^6	0.03	1.461×10^6	1.0
	b_4			0.0005		0.0155	
$\sigma_{S4} / \sigma_M = 0.0005$	n_5					9.920×10^6	0.03
	b_5					0.0005	
	n_6						
	b_6						
	R^2	0.841		0.402		0.402	

Notes

Relative σ values are from Jain et al. (2003). N is the number of OSL components in the fitting equation (Eqn. 2). Initial b_N values for fitting were derived from Jain et al. (2003) (see text). Initial n_N was set to 10^5 and n_N and b_N were constrained to be $n_N > 0$, $b_N > 0$. The number of iterations, step size, and tolerance were set to 10^5, 10^2 and 10^{-500}, respectively. Shaded boxes represent imaginary components with very high *b* and low *n* values (see text for details).

Table 3: *Output parameters of LM-OSL curve fitting of sample ER4 with different numbers of OSL components (initial b values starting from Jain et al.'s (2003) medium component b values)*

	N = 3	N = 4	†N = 4 (0<b<2)
n_1	2.659×10^5	3.980×10^{-4}	1.153×10^5
b_1	0.1224	4.358×10^7	0.3607
n_2	1.478×10^6	2.659×10^5	5.647×10^5
b_2	0.0105	0.1224	0.0302
n_3	1.084×10^7	1.478×10^6	1.292×10^6
b_3	0.0004	0.0105	0.0066
n_4		1.084×10^7	1.215×10^7
b_4		0.0004	0.0003
R^2	0.841	0.841	0.915

† b values obtained by constraining b values to between 0 and 2 were identical to the initial b values used in the fitting process. Shaded boxes represent imaginary components with very high *b* and low *n* values (see text for details).

Table 4: *Output parameters of LM-OSL curve fitting of sample ER4 with different numbers of OSL components (using previous best-fit b values as initial values; $b_1 = 0.3607$, $b_2 = 0.0302$, $b_3 = 0.0066$, $b_4 = 0.0003$, see Table 2 (N = 4))*

TNE9517				ER4			
components	b (s^{-1})	σ (cm^2)	*Relative σ	components	b (s^{-1})	σ (cm^2)	*Relative σ
A	1.4820	2.1×10^{-17}	1.0	a	0.3607	5.1×10^{-18}	1.0
B	0.2580	3.6×10^{-18}	0.2	b	0.0302	4.3×10^{-19}	0.08
C	0.0107	1.5×10^{-19}	0.01	c	0.0066	9.3×10^{-20}	0.02
D	0.0008	1.1×10^{-20}	0.001	d	0.0003	4.2×10^{-21}	0.0008

*Relative σ values were obtained by dividing each σ value with the σ values of components A and a for samples TNE9517 and ER4, respectively.

Table 5: *Photoionisation cross-sections of the OSL components of sample TNE9517 and ER4*

Identification of quartz OSL components in TNE9517 and ER4

The fitting results of the LM-OSL curves for samples TNE9517 (Table 1) and ER4 (Table 4) show the need for 4 OSL components in each case. Provisionally, the separated OSL components are designated as A, B, C, D components for TNE9517, and a, b, c, and d components for ER4, based on the order of appearance of each peak (Table 5 and Fig. 2). Components C and D in TNE9517 are so small that they are barely visible in Fig. 2(a). For ER4, the first three components (a, b, c) appear to have a similar height in the LM-OSL plot (Fig. 2(b)).

The A, B, C, and D components of sample TNE9517 (Fig. 2(a)) can be classified as the fast, medium, slow2, and slow3, components, respectively. Sample ER4 appears not to have either a fast or slow1 OSL component. Thus, components a, b, c and d in Fig. 2(b) can be identified as the medium, slow2, slow3 and slow4 components on the basis of their σ values (Table 5).

Conclusions

In analysing quartz LM-OSL signals, it is important to consider the background count rates during LM-OSL measurements and to ensure that the stimulation power does increase linearly. The background count rates in this study showed a quadratic increase with increasing stimulation power, which might be the result of the combination of the stimulation light breaking through the detection filter and a change in wavelength of the stimulation emission as the power is increased. Direct measurement of the intensity of the light emitted from the blue LEDs confirmed that the power increases linearly during an LM-OSL measurement.

After the subtraction of background count rates, the LM-OSL curves were separated into OSL components using a commercially available software package (SigmaPlot™). The detrapping probabilities were better suited to the mathematical fitting than the photoionisation cross-sections. For TNE9517, a sample with a strong fast component, trying to fit more than 4 components resulted initially in the splitting of the first component (for N=5) and then in the creation of an additional component with an unrealistically high b value (for N=6). Similar problems were encountered for ER4, for which there was no fast component. In this case, using certain initial estimates for the parameters, it was also found necessary to restrict the range of b to between 0 and 2. The detrapping probabilities were used to identify the constituent OSL components. By comparison with published photoionisation cross-sections (Jain et al., 2003), it was shown that the aeolian sample from Tasmania (TNE9517) consists of 4 OSL components (fast, medium, slow 2, and slow 3). The fluvial sample from Kenya (ER4) also has 4 OSL components (medium, slow2, slow3 and slow4), but does not have the fast component. Neither of the samples has a slow1 component.

Acknowledgements

We would like to thank Dr. Mayank Jain for constructive discussions in the early stages of our study, and Bert Roberts for improving the clarity of the paper. JHC was financially supported by a Korea Research Foundation Grant funded by the Korean Government (MOEHRD, Basic Research Promotion Fund, C00265: M01-2004-000-20041-0). GATD acknowledges the support of the NERC through grant NER/T/S/2002/00677.

Appendix 1. Calculation of photoionisation cross-section (σ)

The photoionisation cross-section (σ), which is related to the detrapping probability (b) and the maximum stimulation intensity (I_0) ($b = \sigma I_0$), is a useful parameter for defining the OSL component. While the value of b obtained for a sample will depend upon the maximum intensity of the stimulation light source, the photoionisation cross-section is independent of the measurement conditions. Many authors have reported the photoionisation cross-section of each OSL component obtained using various methods for their samples (Bøtter-Jensen et al., 2003, and references therein). Here, we briefly show the calculation of the photoionisation cross-section from the output parameters (n and b) obtained through mathematical fitting.

The energy (E) of one photon is given by

$$E = h\,v \qquad \text{(Eqn. 3)}$$

where h is Planck's constant, 6.63×10^{-34} J·s = 6.63×10^{-34} W·s^2, and v is frequency (for light with wavelength (λ) of 470 nm, $v = 3 \times 10^8 / 470 \times 10^{-9}$ s^{-1},with $v = c / \lambda$, where c is the speed of light). Thus, the energy of one photon produced by a blue-LED (470 nm) is calculated to be 4.23×10^{-19} W·s. Given that the maximum intensity of the blue-LED array used to measure the LM-OSL curve from samples TNE9517 and ER4 is 30 mW·cm^{-2}, the number of photons per unit time per unit area is 7.1×10^{16} s^{-1}·cm^{-2} (= 0.03 W·cm^{-2} / 4.23×10^{-19} W·s). Then, the photoionisation cross-section, σ, can be obtained by dividing the detrapping probability (b) of each OSL component by the photon flux I_0, i.e. by 7.1×10^{16} s^{-1}·cm^{-2}. The photoionisation cross-sections of each OSL component of samples TNE9517 and ER4 are shown in Table 5.

Appendix 2. Example data sets

So that the reader can try using SigmaPlot™ (ver.7) to deconvolute LM-OSL curves, we have provided the data sets used in this paper. The LM-OSL data for TNE9517 and ER4, after background subtraction, are available as supplementary data from the Ancient TL website (http://www.aber.ac.uk/ancient-tl).

We suggest that you, like us, start with a large number of trapped electrons (n) in each of the traps. So, if you are investigating whether 3 components (N=3) are appropriate, enter $n_1 = 10^5$, $n_2 = 10^5$, and $n_3 = 10^5$. You could equally well try $n = 10^3$, $n = 10^5$, or $n = 10^7$.

For the maximum number of possible iterations, we used 10^5, but you could equally well use a smaller number, e.g. 10^4. The suggested step size is 10^2. The suggested tolerance is 10^{-500}, as discussed in the text.

As a starting point for our measurements taken using blue (λ = 470±30 nm) diode stimulation, the b values for each of the N components are taken as those derived from the photoionisation cross-sections (σ) of Jain et al. (2003). b is related to σ through $b = \sigma I_0$ as detailed in Appendix 1; I_0 is the photon flux for the maximum blue diode stimulation power used to collect the data. Values of b are 1.65, 0.3963, 0.0943, 0.0147, 0.0015 and 0.0002 (s^{-1}) for the fast, medium, slow 1, slow 2, slow 3 and slow 4 components, respectively.

Jain et al. (2003)			Singarayer and Bailey (2003)		
Component	σ cm^2	Relative σ	Component	σ cm^2	Relative σ
Ultrafast	2.9×10^{-16}	13	Ultrafast	7.0×10^{-16}	28
Fast	$(2.32\pm0.16)\times10^{-17}$	1	Fast	$(2.5\pm0.3)\times10^{-17}$	1
Medium	$(5.59\pm0.44)\times10^{-18}$	0.2	Medium	$(5.9\pm2.0)\times10^{-18}$	0.2
Slow 1	$(1.33\pm0.26)\times10^{-18}$	0.06			
Slow 2	$(2.08\pm0.46)\times10^{-19}$	0.01	S_1	$(2.1\pm0.5)\times10^{-19}$	0.01
Slow 3	$(2.06\pm0.16)\times10^{-20}$	0.001	S_2	$(1.2\pm0.2)\times10^{-20}$	0.001
Slow 4	$(2.76\pm0.17)\times10^{-21}$	0.0001	S_3	$(1.9\pm2.9)\times10^{-21}$	0.0001

Table A.1 : *Comparison of published values of σ and the notation used by Jain et al. (2003) and Singarayer and Bailey (2003)*

The same approach can be applied to the deconvolution of any LM-OSL data sets. For measurements made using other stimulation power and/or other stimulation wavelength, different values of *b* will be relevant. For stimulation sources with the same effective wavelength but different powers, the ratio b_M/b_F etc. will be constant. However, the ratio is dependent upon the wavelength, as shown by Singarayer and Bailey (2004).

It should also be remembered that there are two proposed notations for OSL trap identification beyond the fast and medium components, as proposed independently by Singarayer and Bailey (2003) and Jain et al. (2003) on the basis of their LM-OSL measurements on different sedimentary quartz samples. A comparative study of their notation and their values of *σ* are reproduced in Table A.1. In this paper we have adopted the notation of Jain et al. (2003).

Appendix 3. Synthetic LM-OSL data sets

Two additional example data sets are provided and are also available from the Ancient TL website (http://www.aber.ac.uk/ancient-tl). These are synthetic LM-OSL data where the values of *b* and *n* are known, and thus one can assess whether these parameters can be accurately recovered using the fitting procedure proposed in this paper.

Example 1 (Fig. A.1a) is an LM-OSL data set dominated by the fast component; the *n* and *b* values were set to have 93.6% fast, 4.9% medium, 0.8% slow 1, 0.4% slow 2, 0.2% slow 3 and 0.1% slow 4 components in the initial 0.8 s of the CW-OSL signal (Table A.2). Example 2 (Fig. A.1b) is an LM-OSL data set dominated by medium and slow components; the *n* and *b* values were set to have 3.3% fast, 34.7% medium, 7.8% slow 1, 41.3% slow 2, 9.5% slow 3 and 3.4% slow 4 components in the initial 0.8 s of the CW-OSL signal (Table A.3). Also shown in Tables A.2 and A.3 are the results of fitting these data sets using SigmaPlot^{TM}(ver. 7) as described in this paper. In each case, the values of *b* and *n* are recovered accurately.

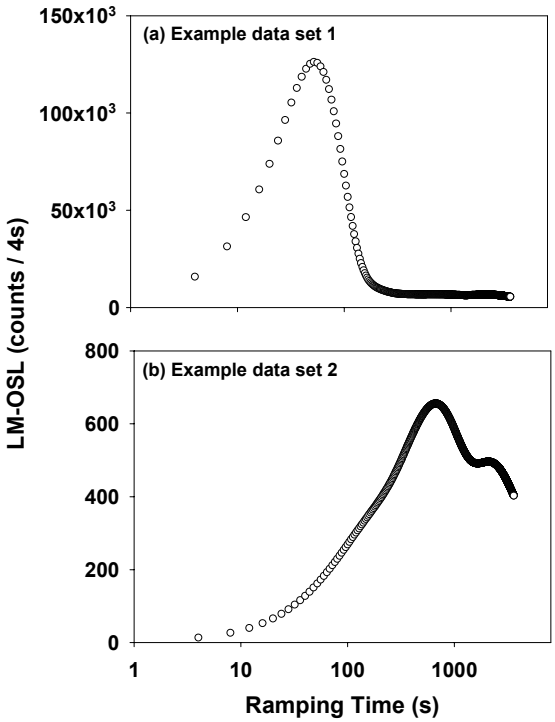

Fig. A.1: *Synthetic LM-OSL data sets used for testing mathematical fitting using SigmaPlot^{TM}. (a) Example data set 1 is dominated (93.6%) by the fast component, and (b) Example data set 2 is dominated by the medium (34.7%) and slow2 (41.3%) components. Details of the parameters used to define these curves are given in Tables A.2 and A.3*

In Table A.4, we tested several sets of initial values for fitting the synthetic data sets. In cases 1-4 (n_1-n_6 were set to 10^5), all the parameters of Example data sets 1 and 2 were successfully recovered, regardless of the initial *b* values tested. However, in cases 5-8 (n_1-n_6 were set to 10^3), the input parameters of Examples 1 and 2 could only be recovered when the initial *b* values were 1 or 0.1. This is rather counter intuitive since the fitting routine is able to fit the data accurately when unrealistic initial starting values of *b* are used, but not when the initial starting values of *b* are very similar to the true values. As was found for the analysis of ER4, constraining the values of *b* to $0 < b < 2$ solves this problem, and allows the correct values to be recovered. Further work is required to understand the cause for this, but it does suggest that researchers should be aware of this problem if their analyses generate values of *b* very different from those which are expected from previously published literature. In such a situation, the analysis should be repeated using a range of initial parameters to test how robust such a conclusion is, and the values of *b* constrained to realistic values.

OSL component	Input parameters		Proportion (%)	Initial parameters		Output parameters (recovered)	
	n_0	b		n_0	b	n_0	b
Fast	9.98×10^{6}	1.3705	93.6	10^5	1.65	$9.98\times10^{6} \pm 4.60\times10^{-4}$	$1.371 \pm 4.13\times10^{-11}$
Medium	1.49×10^{6}	0.3302	4.9	10^5	0.3963	$1.49\times10^{6} \pm 6.19\times10^{-4}$	$0.3302 \pm 2.08\times10^{-10}$
Slow 1	9.45×10^{5}	0.0786	0.8	10^5	0.0943	$9.45\times10^{5} \pm 6.39\times10^{-4}$	$0.0786 \pm 9.59\times10^{-11}$
Slow 2	3.12×10^{6}	0.0123	0.4	10^5	0.0147	$3.12\times10^{6} \pm 1.25\times10^{-3}$	$0.0123 \pm 6.85\times10^{-12}$
Slow 3	1.13×10^{7}	0.00122	0.2	10^5	0.0015	$1.13\times10^{7} \pm 1.03\times10^{-1}$	$0.00122 \pm 5.40\times10^{-12}$
Slow 4	3.25×10^{7}	0.000163	0.1	10^5	0.0002	$3.25\times10^{7} \pm 4.58\times10^{-1}$	$0.000163 \pm 4.52\times10^{-12}$

Table A.2: *Example data set 1 (Modelled LM-OSL data set dominated by fast component). The columns labelled "Input Parameters" show the values of n and b used to generate the modelled LM-OSL data set. Also given are the initial parameters used for fitting the data in SigmaPlot™, and the values of n and b output from SigmaPlot™.*

OSL component	Input parameters		Proportion (%)	Initial parameters		Output parameters (recovered)	
	n_0	b		n_0	b	n_0	b
Fast	4.50×10^{2}	1.3705	3.3	10^5	1.65	$4.50\times10^{2} \pm 4.41\times10^{-5}$	$1.371 \pm 8.79\times10^{-8}$
Medium	1.34×10^{4}	0.3302	34.7	10^5	0.3963	$1.34\times10^{4} \pm 5.93\times10^{-5}$	$0.3302 \pm 2.22\times10^{-9}$
Slow 1	1.14×10^{4}	0.0786	7.8	10^5	0.0943	$1.14\times10^{4} \pm 6.12\times10^{-5}$	$0.0786 \pm 7.62\times10^{-10}$
Slow 2	3.78×10^{5}	0.0123	41.3	10^5	0.0147	$3.78\times10^{5} \pm 1.19\times10^{-4}$	$0.0123 \pm 5.43\times10^{-12}$
Slow 3	8.70×10^{5}	0.00122	9.5	10^5	0.0015	$8.70\times10^{5} \pm 9.88\times10^{-3}$	$0.00122 \pm 6.72\times10^{-12}$
Slow 4	2.34×10^{6}	0.000163	3.4	10^5	0.0002	$2.34\times10^{6} \pm 4.39\times10^{-2}$	$0.000163 \pm 6.01\times10^{-12}$

Table A.3: *Example data set 2 (Modelled LM-OSL data set dominated by medium and slow components). The columns labelled "Input Parameters" show the values of n and b used to generate the modelled LM-OSL data set. Also given are the initial parameters used for fitting the data in SigmaPlot™, and the values of n and b output from SigmaPlot™.*

	n_1-n_6 = 10^5				n_1-n_6 = 10^3			
	Case 1	Case 2	Case 3	Case 4	Case 5	Case 6	Case 7	Case 8
b_1	1.65	1.65	1	0.1	1.65	1.65	1	0.1
b_2	0.3963	0.40	1	0.1	0.3963	0.40	1	0.1
b_3	0.0943	0.09	1	0.1	0.0943	0.09	1	0.1
b_4	0.0147	0.01	1	0.1	0.0147	0.01	1	0.1
b_5	0.0015	0.002	1	0.1	0.0015	0.002	1	0.1
b_6	0.0002	0.0002	1	0.1	0.0002	0.0002	1	0.1
I†	○	○	○	○	×	×	○	○
II†	○	○	○	○	×	×	○	○

† I and II represent Example data sets 1 and 2, respectively.
○Indicates that the *b* and *n* values used to define the synthetic data sets could be recovered.
× Indicates that the *b* and *n* values used to define the synthetic data sets could not be recovered.

Table A.4: *Tests of the ability to recover the known b and n values for Example data sets 1 and 2. Eight different cases were tested, each with a different set of initial parameters used with SigmaPlot™.*

References

Bøtter-Jensen, L., McKeever, S.W.S., Wintle, A.G. (2003) *Optically Stimulated Luminescence Dosimetry*. Elsevier Science, Amsterdam, 355 pp.

Bulur, E. (1996) An alternative technique for optically stimulated luminescence (OSL) experiment. *Radiation Measurements* **26**, 701-709.

Bulur, E., Duller, G.A.T., Solongo, S., Bøtter-Jensen, L., Murray, A.S. (2002) LM-OSL from single grains of quartz: a preliminary study. *Radiation Measurements* **35**, 79-85.

Bulur, E., Bøtter-Jensen, L., Murray, A.S. (2000) Optically stimulated luminescence from quartz measured using the linear modulation technique. *Radiation Measurements* **32**, 407-411.

Choi, J.H., Murray, A.S., Jain, M., Cheong, C.S., Chang, H.W. (2003a) Luminescence dating of well-sorted marine terrace sediments on the southeastern coast of Korea. *Quaternary Science Reviews* **22**, 407-421.

Choi, J.H., Murray, A.S., Cheong, C.S., Hong, D.G., Chang, H.W. (2003b) The resolution of stratigraphic inconsistency in the luminescence ages of marine terrace sediments from Korea. *Quaternary Science Reviews* **22**, 1201-1206.

Choi, J.H., Duller, G.A.T., Wintle, A.G., Cheong, C.S. (in press) Luminescence characteristics of quartz from the southern Kenyan Rift Valley: Dose estimation using LM-OSL SAR. *Radiation Measurements*

Duller, G.A.T., Augustinus, P.C. (in press) Reassessment of the record of linear dune activity in Tasmania using optical dating. *Quaternary Science Reviews*

Jain, M., Murray, A.S., Bøtter-Jensen, L. (2003) Characterisation of blue-light stimulated luminescence components in different quartz samples: implications for dose measurement. *Radiation Measurements* **37**, 441-449.

Kuhns, C.K., Agersnap Larsen, N., McKeever, S.W.S. (2000) Characteristics of LM-OSL from several different types of quartz. *Radiation Measurements* **32**, 413-418.

Singarayer, J.S. (2002) *Linearly modulated optically stimulated luminescence of sedimentary quartz: physical mechanisms and implications for dating.* Unpublished D.Phil. thesis, University of Oxford.

Singarayer, J.S., Bailey, R.M. (2003) Further investigations of the quartz optically stimulated luminescence components using linear modulation. *Radiation Measurements* **37**, 451-458.

Singarayer, J.S., Bailey, R.M. (2004) Component-resolved bleaching spectra of quartz optically stimulated luminescence: preliminary results and implications for dating. *Radiation Measurements* **38**, 111-118.

Tsukamoto, S., Rink, W.J., Watanuki, T. (2003) OSL of tephric loess and volcanic quartz in Japan and an alternative procedure for estimating D_e from a

fast OSL component. *Radiation Measurements* **37**, 459-465.

Yoshida, H., Roberts, R.G., Olley, J.M. (2003) Progress towards single-grain optical dating of fossil mud-wasp nests and associated rock art in northern Australia. *Quaternary Science Reviews* **22**, 1273-1278.

Reviewer

R.G. Roberts

Comments

This is a welcome addition to the luminescence literature, lifting the veil on the practicalities and potential pitfalls of mathematically separating LM-OSL components in quartz. The authors point out several interesting (and unexpected) features of LM-OSL analysis using commercially available software, and highlight the non-routine aspects of this form of data analysis. If LM-OSL signal-separation is to become more widely used as a means of characterising quartz samples or dating them using specific components, then the computational and statistical aspects of LM-OSL analysis need to be placed on a solid footing. This paper begins this process and should stimulate discussion about alternative and improved procedures for teasing apart the different LM-OSL components in quartz and other minerals.